Available online at www.sciencedirect.com
ScienceDirect
Journal of Sound and Vibration 298 (2006) 30–42
JOURNAL OF SOUND AND VIBRATION
www.elsevier.com/locate/jsvi

Non-stationary random ground vibration due to loads moving along a railway track

Feng Lu[a], Qiang Gao[a], J.H. Lin[a,*], F.W. Williams[b]

[a]*State Key Laboratory of Structural Analysis of Industrial Equipment, Dalian University of Technology, Dalian 116023, People's Republic of China*
[b]*Cardiff School of Engineering, Cardiff University, Cardiff CF24 3AA, Wales, UK*

Received 26 May 2005; received in revised form 15 April 2006; accepted 21 April 2006
Available online 7 August 2006

Abstract

The pseudo-excitation method (PEM) and the precise integration algorithm are combined to compute the non-stationary random ground vibration caused by loads moving along a railway track at constant speed. The rails are modeled as a single infinite Euler beam connected to sleepers and hence to ballast. This ballast rests on the ground, which is assumed to consist of layered transversely isotropic soil. The equations of motion of the system are established in a Cartesian coordinate system which moves with the loads. The non-stationary power spectral density and the time-dependent standard deviation can be derived conveniently by means of PEM, while the precise integration algorithm for two-point boundary value problems is applied to the solution of the equations of motion in the frequency/wavenumber domain. By virtue of the transverse isotropic property of the layered soils, the threefold iteration process in the frequency/wavenumber domain is reduced into a twofold iteration process. Hence the computational efficiency is improved considerably.

1. Introduction

Because traffic is becoming faster, traffic-induced ground vibration is receiving increased attention. Since vehicles cause moving random loads they induce non-stationary random vibration at any specific ground location and hence the problem is in general quite difficult to solve.

Due to the limitations of available methods, this problem has been investigated by means of random vibration theory and a variety of different simplifications. The assumption of stationary response was adopted in Refs. [1–3] by neglecting the motion of the loads. Andersen et al. [4] studied a single-degree-of freedom vehicle moving along an infinite beam with random surface irregularities on a Kelvin foundation, with the equations of motion for the system formulated in a coordinate system which moved with the vehicle. Sun and Greenberg [5] presented a follow-up spectral analysis procedure to deal with the dynamic responses of linear systems subjected to moving stochastic sources. Here the responses were assumed to be stationary in

*Corresponding author. Tel.: +86 411 84709403; fax: +86 411 84708400.
E-mail address: jhlin@dlut.edu.cn (J.H. Lin).

0022-460X/$ - see front matter © 2006 Elsevier Ltd. All rights reserved.
doi:10.1016/j.jsv.2006.04.041

a coordinate system which follows the loads and a brief physical explanation was also given. Lombaert et al. [6] proposed a stochastic solution procedure in order to compute the non-stationary free field responses due to a moving load. They derived the autocorrelation function and the time-dependent spectral density at a fixed point in the free field via the Wigner–Ville method. However, when the correlation of loads is taken into account the computational cost becomes very high. The relatively recently developed pseudo-excitation method (PEM) [7–9] provides a new way to solve such problems.

It is known that PEM transforms stationary random analysis into deterministic harmonic analysis, and transforms non-stationary random analysis into deterministic transient analysis. Such transforms are not only highly efficient, but also accurate. For example, Zhong et al. [10] and Gao et al. [11] have studied the propagation of random seismic waves by using PEM. In the present paper the non-stationary PSD functions and the time-dependent standard deviations of the dynamic responses of such a rail system as that described above will be derived by using PEM.

Another issue of interest is how to simulate the propagation of ground waves in stratified soils near the railway track. The transmission of vibration in the vicinity of a rectangular vertical harmonic load located on an elastic layer overlying an infinite elastic half-space was investigated by using a semi-analytical approach [12,13]. Jones and Block [14] proposed an FEM-based scheme to solve Navier's elastodynamic equations. Based on Refs. [12–14], Sheng et al. [15,16] developed a flexibility matrix approach to the solution of the propagation of vibration in ground due to a harmonic load moving along a railway track structure. Recently, Sheng et al. [17] further developed a theoretical model for train-excited ground random vibration due to vertical track irregularities, in which FFT with respect to time was applied so that another sort of PSD was obtained, which does not vary with time. Dieterman and Metrikine [18] and Metrikine and Popp [19] proposed the use of a frequency-dependent "equivalent spring stiffness" as a substitute for the elastic half-space. As an extension of this, Vostroukhov and Metrikine [20] studied the closed-form solutions of the steady-state dynamic responses of a railway track due to a moving train. Lombaert et al. [21] used the Betti–Rayleigh reciprocal theorem to study ground vibration and presented an integral transformation method to improve the computational efficiency. A conventional means for solving wave propagation in stratified media is to transform the partial differential equations into ordinary differential equations (ODEs) in the frequency/wavenumber domain. Zhong [22] proposed use of the precise integration algorithm [23] when investigating this problem and hence he obtained accurate numerical solutions.

PEM is an efficient and exact method for random vibration analysis and the precise integration method is also accurate for solving the ODE. Combining them to analyse the random ground vibration generated by the moving loads yields accurate results. Unfortunately the computational efficiency is still not very satisfactory for complex problems, because of the threefold iteration process in the frequency/wavenumber domain. To overcome this shortcoming, an improved computational procedure is proposed in the present paper, which takes advantage of the transverse isotropic property of the layered soil to reduce the threefold iteration process into a twofold one, by means of a coordinate rotation, while inverse fast fourier transform (IFFT) is applied to obtain the responses in the spatial domain.

2. Non-stationary PSD and time-dependent standard deviation of dynamic responses of a linear system subjected to moving loads

Dynamic properties of linear systems can be characterized by an impulse response function. The impulse response function, $h(\mathbf{x}, \boldsymbol{\xi}; t, s)$, represents the dynamic response at the point, or location $\mathbf{x}$ (which consists of three right-handed Cartesian coordinates) at time t when the system is subjected to an impulse at location $\boldsymbol{\xi}$ and time s. For a time-independent system, the impulse response function degenerates to $h(\mathbf{x}, \boldsymbol{\xi}; t-s)$.

Assume that $p(t)$ is a stationary random load moving along direction $\mathbf{n}$ (again consisting of three right-handed Cartesian coordinates) at speed v and that $\mathbf{V}$ represents the domain occupied by the system. According to the principle of superposition, the transient dynamic response of the system can be written as

$$u(\mathbf{x}, t) = \int_0^t \int_{\mathbf{V}} h(\mathbf{x}, \boldsymbol{\xi}; t-\tau) G(\boldsymbol{\xi} - \mathbf{n}v\tau) p(\tau)\, \mathrm{d}\boldsymbol{\xi}\, \mathrm{d}\tau \tag{1}$$

where $G(\cdot)$ is a unit step function

$$G(\mathbf{x}) = \begin{cases} 1 & \mathbf{x} \in \mathbf{D} \\ 0 & \mathbf{x} \notin \mathbf{D} \end{cases}$$

where $\mathbf{D}$ denotes the finite domain of the load distribution. Using the transformation $\boldsymbol{\xi}' = \boldsymbol{\xi} - \mathbf{n}v\tau$, Eq. (1) can be rewritten as

$$u(\mathbf{x}, t) = \int_0^t h'(\mathbf{x}; t, \tau) p(\tau)\, \mathrm{d}\tau \tag{2}$$

in which $h'(\mathbf{x}; t, \tau) = \int_{\mathbf{D}} h(\mathbf{x}, \boldsymbol{\xi}' + \mathbf{n}v\tau; t - \tau)\, \mathrm{d}\boldsymbol{\xi}'$. By letting each side of Eq. (2) be multiplied by itself and taking the expectation, it is not difficult to obtain the spatial-time correlation function

$$R_u(\mathbf{x}; t_1, t_2) = E[u(\mathbf{x}, t_1) u(\mathbf{x}, t_2)] = \int_0^{t_1} \int_0^{t_2} h'(\mathbf{x}; t_1, \tau_1) h'(\mathbf{x}; t_2, \tau_2) R_p(\tau)\, \mathrm{d}\tau_1\, \mathrm{d}\tau_2 \tag{3}$$

Here $E[\bullet]$ is the expectation operator, $\tau = \tau_1 - \tau_2$, and $R_p(\tau)$ is the autocorrelation functions of $p(t)$. According to Wiener–Khintchine theorem, the relationship between the PSD $S_p(\Omega)$ and the autocorrelation function $R_p(\tau)$ is

$$E[p(\tau_1) p(\tau_2)] = R_p(\tau) = \int_{-\infty}^{+\infty} S_p(\Omega) \mathrm{e}^{\mathrm{i}\Omega(\tau_1 - \tau_2)}\, \mathrm{d}\Omega \tag{4}$$

in which Ω is the frequency and S_p reflects the energy distribution of a stationary random process in the frequency domain. Substituting Eq. (4) into (3), the spatial-time correlation function can be expressed as

$$R_u(\mathbf{x}, t_1, t_2) = \int_{-\infty}^{+\infty} S_p(\Omega) I^*(\mathbf{x}; \Omega, t_1) I(\mathbf{x}; \Omega, t_2)\, \mathrm{d}\Omega \tag{5}$$

$$I(\mathbf{x}; \Omega, t) = \int_0^t h'(\mathbf{x}; t, \tau) \mathrm{e}^{\mathrm{i}\Omega\tau}\, \mathrm{d}\tau \tag{6}$$

where the asterisk denotes complex conjugate.

By letting $t_1 = t_2 = t$, Eq. (5) becomes the time-dependent variance

$$R_u(\mathbf{x}, t) = \sigma_u^2(\mathbf{x}, t) = \int_{-\infty}^{+\infty} S_p(\Omega) I^*(\mathbf{x}; \Omega, t) I(\mathbf{x}; \Omega, t)\, \mathrm{d}\Omega \tag{7}$$

where $R_u(\mathbf{x}, t)$ is variance and $\sigma_u(\mathbf{x}, t)$ is standard deviation. Obviously, the integrand in Eq. (7) is the non-stationary PSD. It can be regarded as the time-dependent distribution of the vibration energy versus frequency at a fixed-point, where

$$S_u(\mathbf{x}, \Omega, t) = S_p(\Omega) I^*(\mathbf{x}; \Omega, t) I(\mathbf{x}; \Omega, t) \tag{8}$$

It is evident from Eq. (6) that $I(\mathbf{x}; \Omega, t)$ is the response of the system due to a unit moving harmonic load $\mathrm{e}^{\mathrm{i}\Omega t}$. Therefore if a pseudo-excitation $\tilde{p}(t) = \sqrt{S_p(\Omega)} \mathrm{e}^{\mathrm{i}\Omega t}$ is used, the corresponding response will be $\tilde{u}(\mathbf{x}, \Omega, t) = \sqrt{S_p(\Omega)} I(\mathbf{x}; \Omega, t)$. Thus

$$S_u(\mathbf{x}, \Omega, t) = \tilde{u}^*(\mathbf{x}, \Omega, t) \tilde{u}(\mathbf{x}, \Omega, t) = S_p(\Omega) I^*(\mathbf{x}; \Omega, t) I(\mathbf{x}; \Omega, t) \tag{9}$$

Thus, the non-stationary PSD of random responses has been derived by PEM.

If steady-state responses are required, solutions can be obtained by changing the lower limit of the integration in Eq. (1) from 0 to $-\infty$. Because the loads are moving, the responses at fixed locations are still non-stationary. Once the deterministic pseudo responses have been worked out, Eqs. (7) and (9) enable the non-stationary PSD functions and time-dependent standard deviations to be obtained both easily and accurately.

3. The equations of motion of the ground and railway track

The structural model is similar to that used in Ref. [16], see Fig. 1. The rails are regarded as a single infinite Euler beam with mass per unit length of track m_r and bending stiffness EI. The sleepers are modeled as a distributed mass m_s per unit length of track. The rail pads are represented by a distributed vertical spring stiffness k_p and the ballast is modeled as an elastic layer with mass m_B and vertical stiffness k_B per unit length of track. The damping properties of all of these track components are accounted for by using complex stiffness parameters.

The ground consists of n layers of soil overlying a rigid foundation. The material constants of the jth layer are identified by Young's modulus E_j, Poisson's ratio v_j, density ρ_j, loss factor η_j and thickness h_j.

When a vehicle moves along a track, its wheelsets are subjected to loads with different time histories. Since such loads are generated by the same track surface, it can reasonably be assumed that if such wheelsets have very similar parameters, the loads will have identical PSD except for certain time lags. In fact, all these loads can be regarded as a generalized single excitation [9]. When dealing with such fully correlated excitations, PEM is still accurate and very efficient. Now, assume that two loads, P_1 and P_2, are moving at speed v along the railway track, and let $\delta(x-vt-x_1)$, $\delta(x-vt-x_2)$ represent their locations. Both loads have the same PSD $S_P(\Omega)$ but with a certain time lag $\tau=(x_1-x_2)/v$. According to PEM [7–9], the pseudo-excitations can be constituted as

$$\tilde{P}_1(t)=\sqrt{S_P(\Omega)}\exp(\mathrm{i}\Omega t),\quad \tilde{P}_2(t)=\sqrt{S_P(\Omega)}\exp(-\mathrm{i}\Omega\tau)\exp(\mathrm{i}\Omega t) \tag{10a}$$

which can be rewritten as the vector

$$\{\tilde{P}\}=\begin{Bmatrix}\tilde{P}_1\\ \tilde{P}_2\end{Bmatrix}=\begin{Bmatrix}1\\ \exp(-\mathrm{i}\Omega\tau)\end{Bmatrix}\sqrt{S_P(\Omega)}\exp(\mathrm{i}\Omega t). \tag{10b}$$

In Eq. (10) the item $\exp(-\mathrm{i}\Omega\tau)$ can be regarded as cross-correlation between P_1 and P_2, and so it is a constant. Therefore it does not increase the computation time. Thus the inclusion of cross-correlation

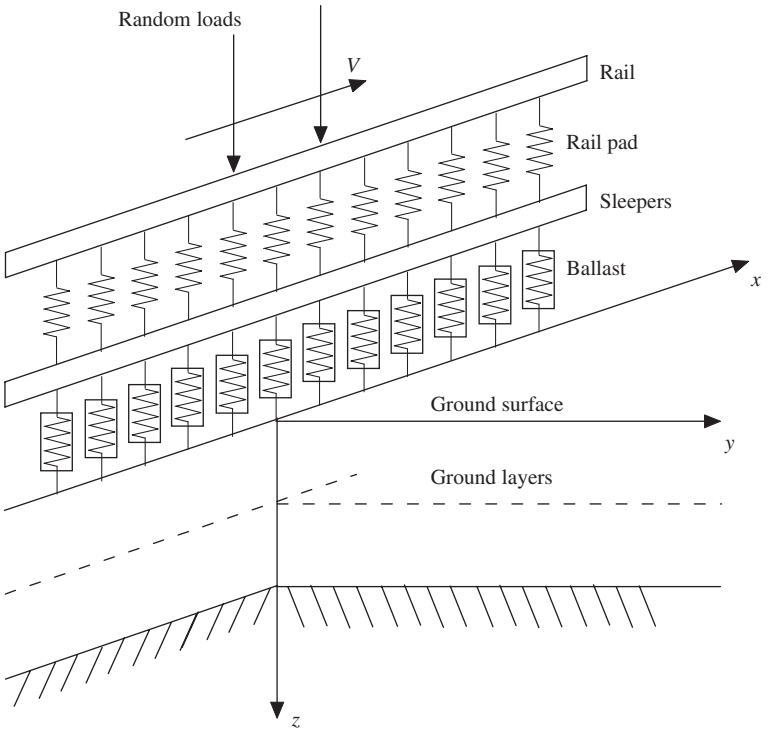

Fig. 1. Model of railway track and ground.

information in PEM is very simple and efficient. For more loads, similar pseudo-excitations can also be constituted. Next, the wave propagation problem due to the deterministic pseudo-excitations of Eq. (10), instead of a few random excitations, needs to be solved.

The railway track is aligned in the x direction and has a contact width $2b$ with the ground. Furthermore, the contact forces are assumed to be normal to the ground surface and uniformly distributed over the width of the track. Referring to Fig. 1, the vertical displacements of the beam, the sleepers and the ground surface directly beneath the beam are denoted by, respectively, $\hat{w}_1(x,t)$, $\hat{w}_2(x,t)$ and $\hat{w}_3(x,t)$. Similarly, the forces at the rail/sleeper, sleeper/ballast and ballast/ground interfaces are denoted by $\hat{F}_1(x,t), \hat{F}_2(x,t)$ and $\hat{F}_3(x,t)$, while the displacements of the jth soil layer in x, y and z directions are $\hat{u}_j(x,y,z,t), \hat{v}_j(x,y,z,t)$ and $\hat{w}_j(x,y,z,t)$.

A local right-hand Cartesian coordinate system which follows the moving loads is introduced by the transformation $\chi = x - vt$. Due to convection the partial derivative with respect to time in the moving frame of reference includes a spatial derivative

$$\left.\frac{\partial}{\partial t}\right|_{\chi} = \left.\frac{\partial}{\partial t}\right|_{x} + v\frac{\partial}{\partial \chi} \tag{11}$$

Now let $\dot{w} = \partial\hat{w}/\partial t\big|_{\chi}$ and $\ddot{w} = \partial^2\hat{w}/\partial t^2\big|_{\chi}$. Then the differential equations of the system (except for the ground) in the local coordinates are given by Eqs. (12)–(14) which apply, respectively, to the beam, the sleepers and the ballast layer, for which a consistent mass approximation is used.

$$EI\frac{\partial^4\hat{w}_1}{\partial\chi^4} + m_r\left(\ddot{\hat{w}}_1 - 2v\frac{\partial\dot{\hat{w}}_1}{\partial\chi} + v^2\frac{\partial^2\hat{w}_1}{\partial\chi^2}\right) + \hat{F}_1 = \tilde{P}_1(t)\delta(\chi - x_1) + \tilde{P}_2(t)\delta(\chi - x_2). \tag{12}$$

$$\hat{F}_1 = k_p(\hat{w}_1 - \hat{w}_2)$$

$$m_s\left(\ddot{\hat{w}}_2 - 2v\frac{\partial\dot{\hat{w}}_2}{\partial\chi} + v^2\frac{\partial^2\hat{w}_2}{\partial\chi^2}\right) - \hat{F}_1 + \hat{F}_2 = 0 \tag{13}$$

$$\frac{m_B}{6}\begin{bmatrix}2 & 1\\ 1 & 2\end{bmatrix}\left(\begin{Bmatrix}\ddot{\hat{w}}_2\\ \ddot{\hat{w}}_3\end{Bmatrix} - 2v\begin{Bmatrix}\partial\dot{\hat{w}}_2/\partial\chi\\ \partial\dot{\hat{w}}_3/\partial\chi\end{Bmatrix} + v^2\begin{Bmatrix}\partial^2\hat{w}_2/\partial\chi^2\\ \partial^2\hat{w}_3/\partial\chi^2\end{Bmatrix}\right) + k_B\begin{bmatrix}1 & -1\\ -1 & 1\end{bmatrix}\begin{Bmatrix}\hat{w}_2\\ \hat{w}_3\end{Bmatrix} + \begin{Bmatrix}-\hat{F}_2\\ \hat{F}_3\end{Bmatrix} = 0 \tag{14}$$

Meanwhile, the differential equations of the $j$thlayer of the ground are

$$\begin{aligned}
(\lambda_j + G_j)\tfrac{\partial\Delta_j}{\partial\chi} + G_j\nabla^2\hat{u}_j &= \rho_j\left(\ddot{\hat{u}}_j - 2v\tfrac{\partial\dot{\hat{u}}_j}{\partial\chi} + v^2\tfrac{\partial^2\hat{u}_j}{\partial\chi^2}\right),\\
(\lambda_j + G_j)\tfrac{\partial\Delta_j}{\partial\chi} + G_j\nabla^2\hat{v}_j &= \rho_j\left(\ddot{\hat{v}}_j - 2v\tfrac{\partial\dot{\hat{v}}_j}{\partial\chi} + v^2\tfrac{\partial^2\hat{v}_j}{\partial\chi^2}\right),\\
(\lambda_j + G_j)\tfrac{\partial\Delta_j}{\partial\chi} + G_j\nabla^2\hat{w}_j &= \rho_j\left(\ddot{\hat{w}}_j - 2v\tfrac{\partial\dot{\hat{w}}_j}{\partial\chi} + v^2\tfrac{\partial^2\hat{w}_j}{\partial\chi^2}\right),
\end{aligned} \tag{15}$$

where ∇^2 is the Laplace operator, λ_j and G_j are the Lamé constants and

$$\lambda_j = \frac{v_jE_j(1 + i\eta_j\,\mathrm{sgn}(\Omega))}{(1+v_j)(1-2v_j)}, \quad G_j = \frac{E_j(1 + i\eta_j\,\mathrm{sgn}(\Omega))}{2(1+v_j)},$$
$$\Delta_j = \frac{\partial\hat{u}_j}{\partial\chi} + \frac{\partial\hat{v}_j}{\partial y} + \frac{\partial\hat{w}_j}{\partial z}.$$

Transforming Eqs. (12)–(15) into the frequency/wavenumber $(\Omega, \kappa_\chi, \kappa_y)$ domain gives

$$\begin{bmatrix} EI\kappa_\chi^4 - \omega^2m_r + k_p & -k_p & 0\\ -k_p & k_p + k_B - \omega^2(m_s + m_B/3) & -(k_B + \omega^2m_B/6)\\ 0 & -(k_B + \omega^2m_B/6) & (k_B - \omega^2m_B/3)\end{bmatrix}\begin{Bmatrix}w_1\\ w_2\\ w_3\end{Bmatrix} = \begin{Bmatrix}P\\ 0\\ -F_3\end{Bmatrix} \tag{16}$$

$$P = \sqrt{S_P(\Omega)}[\exp(-i\kappa_\chi x_1) + \exp(-i\kappa_\chi x_2)\exp(-i\Omega\tau)]$$

$$\mathbf{K}_{22}\mathbf{q}'' + (\mathbf{K}_{21} - \mathbf{K}_{12})\mathbf{q}' - (\mathbf{K}_{11} - \rho\omega^2\mathbf{I})\mathbf{q} = \mathbf{0} \tag{17}$$

$$\mathbf{K}_{22} = \begin{bmatrix} G_j & 0 & 0 \\ 0 & G_j & 0 \\ 0 & 0 & \lambda_j + 2G_j \end{bmatrix}$$

$$\mathbf{K}_{21} = -\mathbf{K}_{12}^{\mathrm{T}} = \mathrm{i}\kappa_\chi \begin{bmatrix} 0 & 0 & G_j \\ 0 & 0 & 0 \\ \lambda_j & 0 & 0 \end{bmatrix} + \mathrm{i}\kappa_y \begin{bmatrix} 0 & 0 & 0 \\ 0 & 0 & G_j \\ 0 & \lambda_j & 0 \end{bmatrix}$$

$$\mathbf{K}_{11} = \kappa_\chi^2 \begin{bmatrix} \lambda_j + 2G_j & 0 & 0 \\ 0 & G_j & 0 \\ 0 & 0 & G_j \end{bmatrix} + \kappa_y^2 \begin{bmatrix} G_j & 0 & 0 \\ 0 & \lambda_j + 2G_j & 0 \\ 0 & 0 & G_j \end{bmatrix} + \kappa_\chi\kappa_y \begin{bmatrix} 0 & \lambda_j + G_j & 0 \\ \lambda_j + G_j & 0 & 0 \\ 0 & 0 & 0 \end{bmatrix}$$

in which: $\mathbf{I}$ is the (3×3) identity matrix; $\mathbf{q} = \{u_j, v_j, w_j\}^{\mathrm{T}}$, $\omega = \Omega - v\kappa_\chi$ (Ω is the frequency of vibration in the fixed frame of reference whereas ω can be regarded as the circular frequency in the moving frame of reference) and $(\#)' = \partial(\#)/\partial z$ represents differentiation with respect to z. Eqs. (16) and (17) are the governing equations of the coupling system. In the following section, Eq. (17) will be solved by using the precise integration method.

4. Solution of the coupling system

4.1. The interval formulation for the ground

Assume that the jth layer of the ground is in the interval $[z_a, z_b]$ and define a dual vector

$$\mathbf{p} = \{\tau_{xz}, \tau_{yz}, \sigma_z\}^{\mathrm{T}} = \mathbf{K}_{22}\mathbf{q}' + \mathbf{K}_{21}\mathbf{q} \tag{18}$$

which represents the traction vector. Then Eq. (17) can be rewritten in the state space as

$$\mathbf{v}' = \mathbf{H}\mathbf{v}, \quad \mathbf{H} = \begin{bmatrix} \mathbf{AD} \\ \mathbf{BC} \end{bmatrix}, \quad \mathbf{v} = \begin{Bmatrix} \mathbf{q} \\ \mathbf{p} \end{Bmatrix} \tag{19}$$

$$\mathbf{A} = -\mathbf{K}_{22}^{-1}\mathbf{K}_{21}, \quad \mathbf{B} = \mathbf{K}_{11} - \mathbf{K}_{12}\mathbf{K}_{22}^{-1}\mathbf{K}_{21} - \rho\omega^2\mathbf{I},$$
$$\mathbf{C} = \mathbf{K}_{12}\mathbf{K}_{22}^{-1}, \quad \mathbf{D} = \mathbf{K}_{22}^{-1}.$$

From Eq. (19), the interval formulation of the jth layer can be obtained as

$$\mathbf{q}_b = \mathbf{F}\mathbf{q}_a - \mathbf{G}\mathbf{p}_b, \quad \mathbf{p}_a = \mathbf{Q}\mathbf{q}_a + \mathbf{E}\mathbf{p}_b \tag{20}$$

where $\mathbf{q}_a$ and $\mathbf{q}_b$ represent the displacement vectors and $\mathbf{p}_a$ and $\mathbf{p}_b$ represent the traction vectors at the two sides of the jth layer and $\mathbf{F}, \mathbf{G}, \mathbf{Q}$ and $\mathbf{E}$ satisfy the following relations and the boundary conditions. (more detail can be found in Ref. [10]).

$$\mathbf{F}' = (\mathbf{A} + \mathbf{GB})\mathbf{F}, \quad \mathbf{E}' = \mathbf{E}(\mathbf{BG} - \mathbf{C})$$
$$\mathbf{G}' = \mathbf{AG} - \mathbf{GC} - \mathbf{D} + \mathbf{GBG}, \quad \mathbf{Q}' = -\mathbf{EBF} \tag{21a}$$

$$\mathbf{G}(z_a, z_b) = \mathbf{Q}(z_a, z_b) = \mathbf{0}, \ \mathbf{F}(z_a, z_b) = \mathbf{E}(z_a, z_b) = \mathbf{I} \text{ when } z_a \to z_b. \tag{21b}$$

Consider two adjacent intervals $[z_a, z_b]$ and $[z_b, z_c]$. Applying Eq. (20) to them gives

$$\mathbf{q}_b = \mathbf{F}_1\mathbf{q}_a - \mathbf{G}_1\mathbf{p}_b,\ \mathbf{p}_a = \mathbf{Q}_1\mathbf{q}_a + \mathbf{E}_1\mathbf{p}_b \text{ for } [z_a, z_b], \tag{22a,b}$$

$$\mathbf{q}_c = \mathbf{F}_2\mathbf{q}_b - \mathbf{G}_2\mathbf{p}_c,\ \mathbf{p}_b = \mathbf{Q}_2\mathbf{q}_b + \mathbf{E}_2\mathbf{p}_c \text{for } [z_b, z_c], \tag{22c,d}$$

The intervals $[z_a, z_b]$ and $[z_b, z_c]$ can be merged into the interval $[z_a, z_c]$, see Ref. [23], to give

$$\begin{aligned}
&\mathbf{q}_c = \mathbf{F}_c\mathbf{q}_a - \mathbf{G}_c\mathbf{p}_c,\ \mathbf{p}_a = \mathbf{Q}_c\mathbf{q}_a + \mathbf{E}_c\mathbf{p}_c \text{ for } [z_a, z_c],\\
&\mathbf{F}_c = \mathbf{F}_2(\mathbf{I} + \mathbf{G}_1\mathbf{Q}_2)^{-1}\mathbf{F}_1,\ \mathbf{G}_c = \mathbf{G}_2 + \mathbf{F}_2(\mathbf{G}_1^{-1} + \mathbf{Q}_2)^{-1}\mathbf{E}_2,\\
&\mathbf{Q}_c = \mathbf{Q}_1 + \mathbf{E}_1(\mathbf{Q}_2^{-1} + \mathbf{G}_1)^{-1}\mathbf{F}_1,\ \mathbf{E}_c = \mathbf{E}_1(\mathbf{I} + \mathbf{Q}_2\mathbf{G}_1)^{-1}\mathbf{E}_2.
\end{aligned} \tag{23}$$

By combining all of the elastic layers and by assuming that the ground overlies an absolutely rigid foundation, the whole interval formulation for the ground can be written as

$$\mathbf{q}_{\text{up}} = \bar{\mathbf{G}}\mathbf{p}_{\text{up}} \tag{24}$$

in which $\mathbf{q}_{\text{up}} = \{u_{\text{up}}, v_{\text{up}}, w_{\text{up}}\}^{\text{T}}$ and $\mathbf{p}_{\text{up}} = \{\tau_{xz}, \tau_{yz}, \sigma_z\}^{\text{T}}$ represent the displacement and traction vectors at the ground surface, respectively, and $\bar{\mathbf{G}}$ is the total coefficient matrix.

4.2. Solution of the coupling system

Continuity of displacement at the ground surface is expressed as [15]

$$w_3(\kappa_\chi, \Omega) = \frac{1}{2\pi}\int_{-\infty}^{+\infty} w_{\text{up}}(\kappa_\chi, \kappa_y, \Omega)\mathrm{e}^{\mathrm{i}\kappa_y y}\,\mathrm{d}\kappa_y|_{y=0} = \frac{1}{2\pi}\int_{-\infty}^{+\infty} w_{\text{up}}(\kappa_\chi, \kappa_y, \Omega)\,\mathrm{d}\kappa_y \tag{25}$$

and force equilibrium at the ground surface is expressed as [15]

$$\tau_{xz}^{\text{up}} = 0,\ \tau_{yz}^{\text{up}} = 0,\ \sigma_z^{\text{up}} = \frac{\sin(\kappa_y b)}{\kappa_y b}F_3(\kappa_\chi, \Omega) \tag{26}$$

Substituting Eq. (26) into Eqs. (24) and (25) gives

$$w_3(\kappa_\chi, \Omega) = L(\kappa_\chi, \Omega)F_3(\kappa_\chi, \Omega), \tag{27}$$

where

$$L(\kappa_\chi, \Omega) = -\frac{1}{2\pi}\int_{-\infty}^{+\infty} \bar{\mathbf{G}}_{33}(\Omega - v\kappa_\chi, \kappa_\chi, \kappa_y)\frac{\sin(\kappa_y b)}{\kappa_y b}\,\mathrm{d}\kappa_y.$$

Eq. (27) is substituted into Eq. (16) to calculate F_3, which is then substituted into Eq. (24) to produce the dynamic responses of the ground surface, i.e. $u(\kappa_\chi, \kappa_y, \Omega)$, $v(\kappa_\chi, \kappa_y, \Omega)$ and $w(\kappa_\chi, \kappa_y, \Omega)$. By using the IFFT and the transformation $x = \chi + vt$, the responses $\hat{u}(x, y, \Omega, t)$, $\hat{v}(x, y, \Omega, t)$ and $\hat{w}(x, y, \Omega, t)$ in the fixed coordinate system can be obtained. Then by using PEM, the non-stationary PSDs $S_u(x, y, \Omega, t)$, $S_v(x, y, \Omega, t)$ and $S_w(x, y, \Omega, t)$ and the time-dependent standard deviations $\sigma_u(x, y, t)$, $\sigma_v(x, y, t)$ and $\sigma_w(x, y, t)$ can be computed from

$$\begin{aligned}
&S_u(x, y, \Omega, t) = \hat{u} \bullet \hat{u}^*, \quad S_v(x, y, \Omega, t) = \hat{v} \bullet \hat{v}^*, \quad S_w(x, y, \Omega, t) = \hat{w} \bullet \hat{w}^*\\
&\sigma_u^2(t) = \int_{-\infty}^{+\infty} S_u\,\mathrm{d}\Omega, \quad \sigma_v^2(t) = \int_{-\infty}^{+\infty} S_v\,\mathrm{d}\Omega, \quad \sigma_w^2(t) = \int_{-\infty}^{+\infty} S_w\,\mathrm{d}\Omega
\end{aligned} \tag{28}$$

5. Strategy to accelerate the computation

The above section has given the computation process. When a group of $(\Omega, \kappa_\chi, \kappa_y)$ is specified, the matrix $\bar{\mathbf{G}}(\omega = \Omega - v\kappa_\chi, \kappa_\chi, \kappa_y)$ has to be calculated. It contains a threefold integration process and so is very time consuming. Therefore it is very desirable to accelerate the computation. To achieve this, a strategy based on

a coordinate system rotation follows. The properties of matrix $\bar{\mathbf{G}}$ are the foundation of this strategy, which was also discussed in Ref. [15].

Firstly, let a new coordinate system $(\kappa'_\chi, \kappa'_y)$ be established, which shares the origin of the coordinate system (κ_χ, κ_y). Secondly, let a series of $\omega' \in [0, \max(\Omega - v\kappa_\chi)]$ and $\kappa'_\chi \in \left[0, \max(\sqrt{\kappa_\chi^2 + \kappa_y^2})\right]$ be selected, with $\kappa'_y = 0$. Here we let the lower limit of ω' be zero, because $\bar{\mathbf{G}}(-\omega', \kappa'_\chi, 0)$ can be obtained easily from $\bar{\mathbf{G}}(\omega', \kappa'_\chi, 0)$. Thirdly, let the corresponding $\bar{\mathbf{G}}' = \bar{\mathbf{G}}(\omega', \kappa'_\chi, 0)$ be computed and save these matrices. As the contact force is vertical, only the third column of $\bar{\mathbf{G}}'$ is required, which enables computer storage space to be saved. The procedure for computing matrix $\bar{\mathbf{G}}(\Omega, \kappa_\chi, \kappa_y)$ is (1) rotate the coordinates $(\kappa'_\chi, \kappa'_y)$ and let the κ'_χ axis pass the point (κ_χ, κ_y); (2) select the matrix $\bar{\mathbf{G}}' = \bar{\mathbf{G}}(\omega' = \Omega - v\kappa_\chi, \kappa'_\chi = \sqrt{\kappa_\chi^2 + \kappa_y^2}, 0)$ (may be $\bar{\mathbf{G}}'$ cannot be obtained completely accurately, but an approximation with sufficient precision can be found) and; (3) compute the matrix $\bar{\mathbf{G}} = \mathbf{T}^{\mathrm{T}}\bar{\mathbf{G}}'\mathbf{T}$ using the coordinate transform matrix $\mathbf{T}$.

6. Numerical examples

The parameters of the ground and the railway track are listed in Tables 1 and 2 [15].

Example 1. In order to test the correctness of the program, some of its results were compared with those of Ref. [15]. The method of separation of variables [24] was applied to deal with the elastic half-space in Ref. [15] and the load used was a unit harmonic excitation with frequency 40 Hz. Fig. 2 presents the distribution of the vertical ground displacement in the wavenumber domain due to unit harmonic load intensity acting on a 2.7 m × 2.7 m rectangle on the ground. Fig. 3 presents the distributions of the longitudinal, lateral and vertical ground displacements due to unit harmonic load acting on the track at the origin.

In Fig. 2 the amplitudes decay to zero beyond the wavenumbers $\kappa_\chi = 2.3\ \mathrm{rad\,m^{-1}}$ or $\kappa_y = 2.3\ \mathrm{rad\,m^{-1}}$, which agree well with the results shown in Ref. [15]. In addition, the shapes of the ground displacement distribution in Fig. 3 are quite similar to those shown in Ref. [15]. These, and additional checks not reported here, verify the appropriateness of the method and program developed for this paper.

Example 2. Random vibration of the vehicle/track coupling system was extensively investigated in Chapter 3 of Ref. [25], in which a vehicle/track-coupling model was set up and the PSDs of the vehicle load were obtained at speed $44.44\ \mathrm{m\,s^{-1}}$. The same model is used as the present example except that the speed is higher,

Table 1
The parameters for the ground

Layer	Depth (m)	Young's modulus ($10^6\,\mathrm{N\,m^{-2}}$)	Poisson ratio	Density ($\mathrm{kg\,m^{-3}}$)	Loss factor
1	7	269	0.257	1550	0.1
2	150	2040	0.179	2450	0.1

Table 2
The parameters for the railway track

Mass of rail beam per unit length of track $120\,\mathrm{kg\,m^{-1}}$
Bending stiffness of rail beam $1.26 \times 10^7\,\mathrm{N\,m^{-2}}$
Rail pad stiffness $3.5 \times 10^8\,\mathrm{N\,m^{-2}}$
Rail pad loss factor 0.15
Mass of sleeper per unit length of track $490\,\mathrm{kg\,m^{-1}}$
Mass of ballast per unit length of track $1200\,\mathrm{kg\,m^{-1}}$
Ballast stiffness per unit length of track $3.15 \times 10^8\,\mathrm{N\,m^{-2}}$
Loss factor of ballast 1.0
Contact width of railway and ground 2.7 m

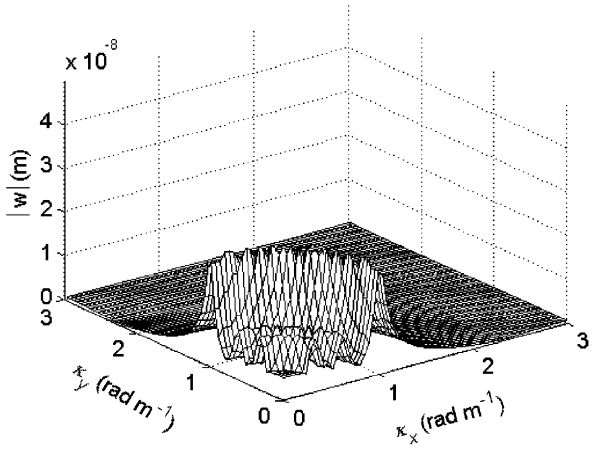

Fig. 2. Vertical ground displacement due to unit ground excitation.

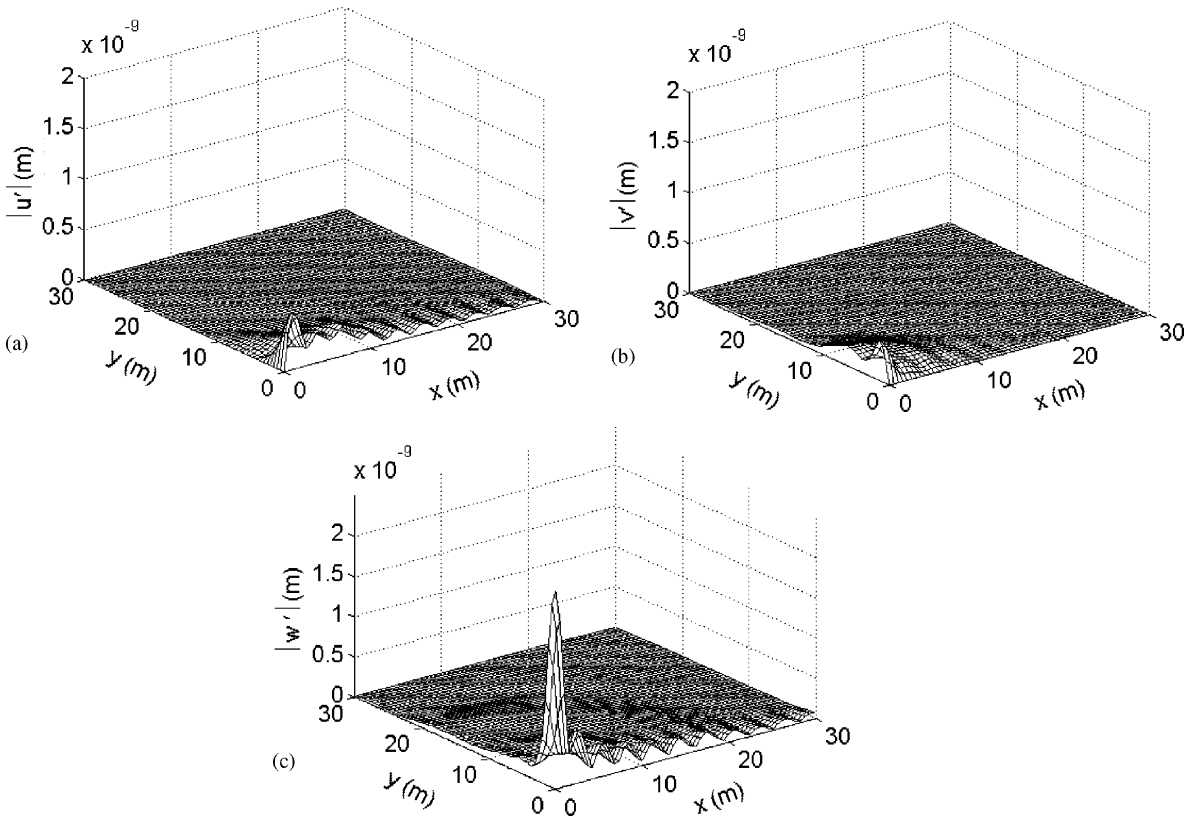

Fig. 3. Ground displacement components due to unit vehicle load: (a) longitudinal; (b) lateral and; (c) vertical.

because no other PSD data are available as vehicle random loads. It is noted that when the IFFT is used, care must be taken to ensure both that at each wavenumber point $\bar{\mathbf{G}}(\Omega, \kappa_\chi, \kappa_y)$ there is sufficient precision and also that there are sufficient points for the transformation to give a sufficiently accurate quadrature. In this example 1000 points were taken κ'_x, ranging from 0 to 10 rad m^{-1}, and the IFFT was carried out over a grid of 512×256 within $-5 < \kappa_\chi, \kappa_y < 5$ rad m^{-1}. The frequency ω varies with the wavenumber κ_χ according to $\omega = \Omega - v\kappa_\chi$, and the influence of κ_χ on various results was remarkably high. Therefore κ_χ should be expressed by mean of a suitably dense grid.

Two fixed locations (0,15 m) and (0,25 m) were chosen when evaluating the vibration status, where location (x, y) represents a ground surface point with coordinates x m and y m. Thus the first location is closer to the track. Fig. 4 shows the non-stationary PSD of the vertical displacements of these two locations due to a single load moving along the track at speeds of 50, 75 and 100 m/s. It is assumed that when $t = 0$ the moving load passes the origin (0,0). Obviously material damping becomes more significant at the higher frequencies, whereas geometrical damping dominates at lower frequencies. Comparing Figs. 4(a) and (b), it can be seen that the vibration energy at location (0,15) is distributed approximately within the frequency range from a few Hz to 100 Hz, whereas at (0,25) the range becomes from a few Hz to 80 Hz. Therefore, the vibration energy is distributed in higher frequencies in regions closer to the track. Figs. 4(a) and (b) reflect this phenomenon reasonably. Figs. 4(c)–(f) show that when the load passes the observation locations progressively more quickly, the vibration energy increases remarkably and is concentrated within the range from a few Hz up to 50 Hz, moreover there are secondary peaks which corresponded to the load speed.

The time-dependent standard deviations of the vertical displacements at the speeds of 50 and 100 m/s are shown in Fig. 5, for the locations (0,15), (0,25) and (0,35), respectively. Clearly, when the load is far from these three locations their displacement responses are of similar magnitude, wheres as the load passes by them their vibration levels differ substantially.

Example 3. Four vehicle loads act on the track at the locations $x_1 = 10.2$ m, $x_2 = 7.8$ m, $x_3 = -7.8$ m and $x_4 = -10.2$ m [25]. It is assumed that these loads are fully correlated, but that time lags exist between them, which can be expressed as

$$\{P_1(t), P_2(t), P_3(t), P_4(t)\}^{\mathrm{T}} = \{P(t-\tau_1), P(t-\tau_2), P(t-\tau_3), P(t-\tau_4)\}^{\mathrm{T}}$$

$$\tau_i = (x_1 - x_i)/vi = 1, 2, 3, 4$$

The time-dependent standard deviations of the vertical displacement at locations (0,15) and (0,25) due to the above four loads moving at speeds of 50 and 100 m s^{-1} are shown in, respectively, Figs. 6 and 7. The solid and dotted curves represent, respectively, the results with or without account being taken of the cross-correlation between the loads. Clearly the influence of the cross-correlation trends towards being negligible at speed 50 m/s^{-1}, whereas when the speed increases to 100 m/s the responses when cross-correlation is neglected are

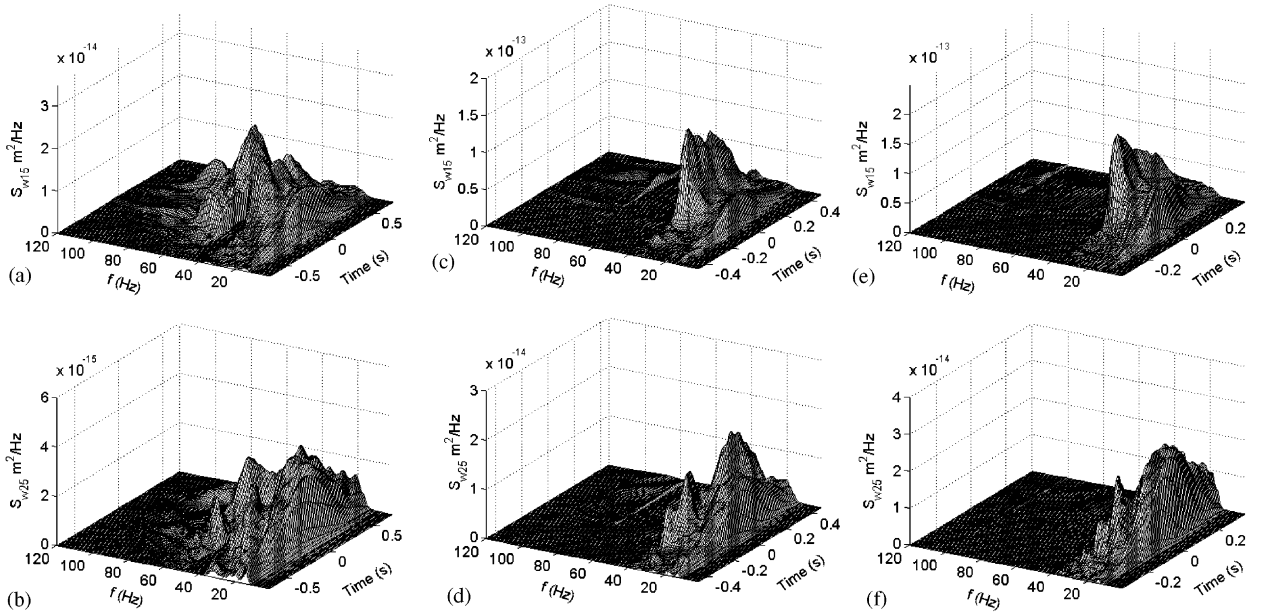

Fig. 4. Non-stationary PSD of vertical displacements for the locations and train velocities shown. (a) The location (0,15), $v = 50$ m s^{-1}; (b) the location (0,25), $v = 50$ m s^{-1}; (c) the location (0,15), $v = 75$m s^{-1}; (d) the location (0,25), $v = 75$ m s^{-1}; (e) the location (0,15), $v = 100$ m s^{-1}; (f) the location (0,25); $v = 100$ m s^{-1}.

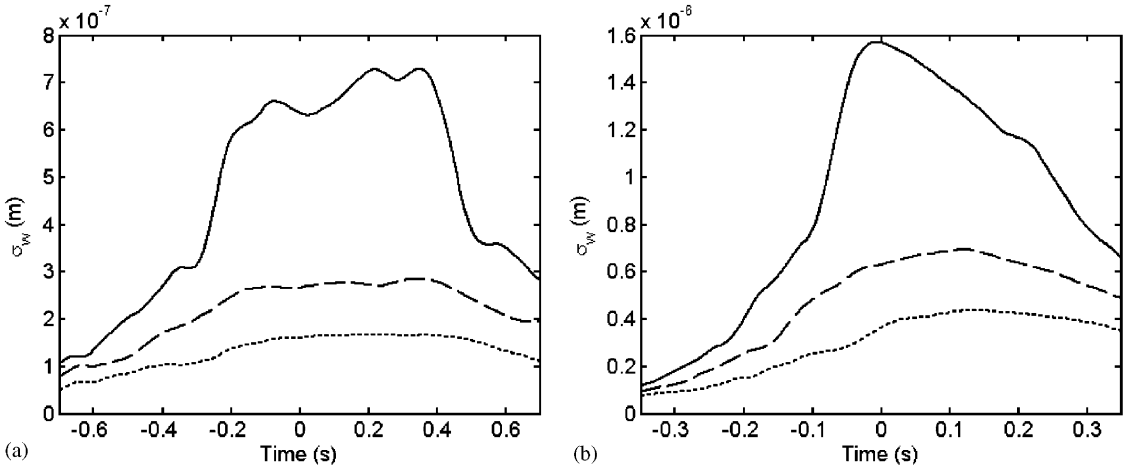

Fig. 5. Time-dependent standard deviation of vertical displacement at the locations (0,15) (————), (0,25) (- - - - -) and (0,35) (- - - - -) for: (a) $v = 50\,\mathrm{m\,s^{-1}}$ and; (b) $v = 100\,\mathrm{m\,s^{-1}}$.

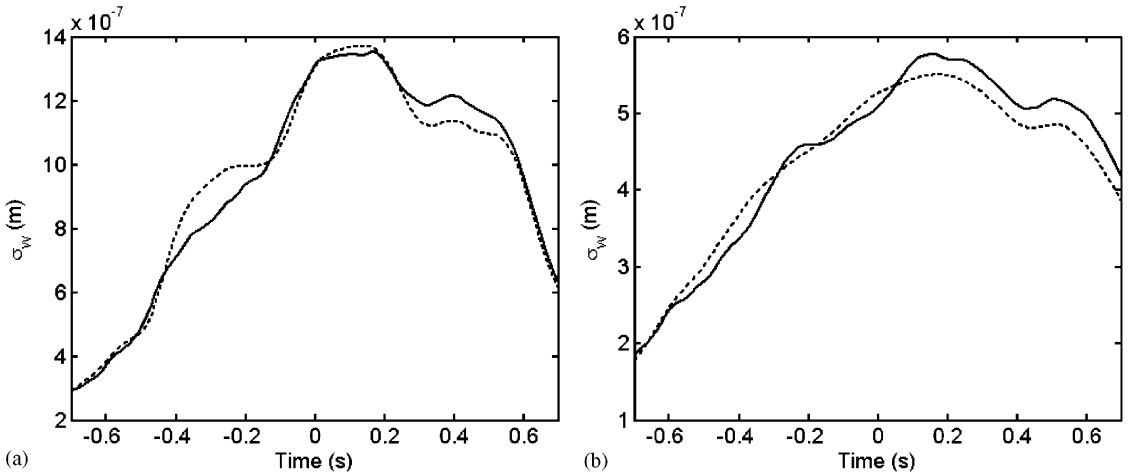

Fig. 6. Time-dependent standard deviation of vertical displacement, either including (————) or neglecting (- - - - -) cross-correlation, when $v = 50\,\mathrm{m\,s^{-1}}$ and at location: (a) (0, 15) and; (b) (0, 25).

much higher than when it is included. In the well known special case that the two loads act at the same location, according to random vibration theory the standard deviation when cross-correlation is considered will be $\sqrt{2}$ times as high as when it is neglected. Hence, it can be concluded that as conditions differ, accounting for cross-correlation can either increase or decrease responses. Because including cross-correlation does not add to the computation time when using PEM, cross-correlation can always be taken into account.

7. Conclusions

The non-stationary ground random vibration generated by random loads moving along a railway track at a constant speed is investigated by the new algorithm proposed, which is based on the PEM and the precise integration algorithm. The PEM formulas for time-dependent PSDs and standard deviations are derived for the coupled vehicle–track systems subjected to moving random loads. An acceleration scheme has been provided which reduces the computational effort considerably. Numerical examples accord reasonably with some phenomenon. Numerical examples also show that as conditions differ, accounting for cross-correlation

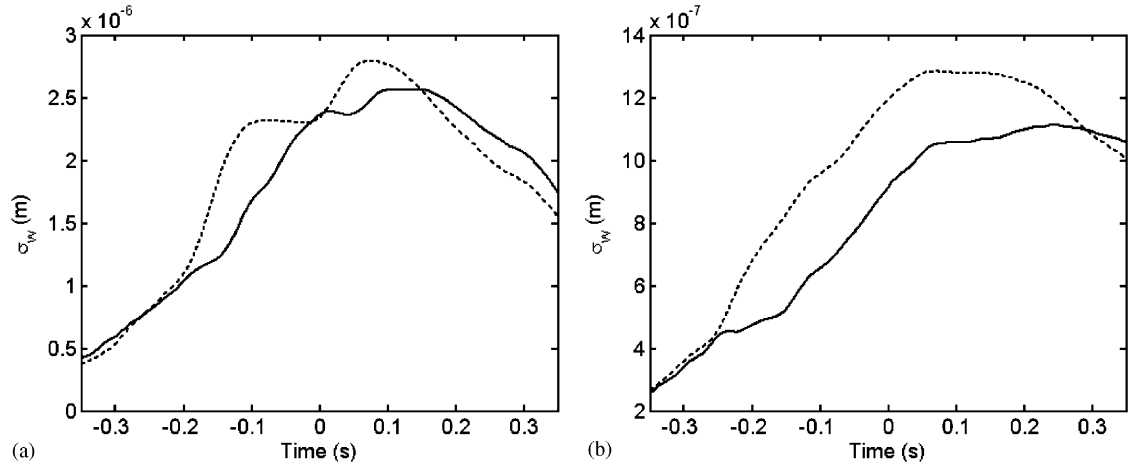

Fig. 7. Time-dependent standard deviation of vertical displacement, either including (————) or neglecting (-----) cross-correlation, when $v = 100\,\mathrm{m\,s^{-1}}$ and at location: (a) (0, 15) and; (b) (0, 25).

can either increase or decrease responses. Because including cross-correlation does not add to the computation time when using PEM, cross-correlation can always be taken into account.

Acknowledgement

The authors are grateful for support from the National Natural Science Foundation of China (Grant no 10472023); the doctoral research fund of the Chinese Ministry of Education (Grant no 20040141020) and; the Cardiff Advanced Chinese Engineering Centre.

References

[1] H.E.M. Hunt, Stochastic modelling of traffic-induced ground vibration, *Journal of Sound and Vibration* 144 (1991) 53–70.
[2] H.E.M. Hunt, Modelling of road vehicles for calculation of traffic-induced vibration as a random process, *Journal of Sound and Vibration* 144 (1991) 41–51.
[3] H.E.M. Hunt, Modelling of rail vehicles and track for calculation of ground-vibration transmission into buildings, *Journal of Sound and Vibration* 193 (1996) 185–194.
[4] L. Andersen, S.R.K. Nielsen, P.H. Kirkegaard, Finite element modelling of infinite Euler beams on Kelvin foundations exposed to moving loads in convected co-ordinates, *Journal of Sound and Vibration* 241 (2001) 587–604.
[5] L. Sun, B.S. Greenberg, Dynamic response of linear systems to moving stochastic sources, *Journal of Sound and Vibration* 229 (2000) 957–972.
[6] G. Lombaert, G. Degrande, D. Clouteau, The non-stationary freefield response for a moving load with a random amplitude, *Journal of Sound and Vibration* 278 (2004) 611–635.
[7] J.H. Lin, Y. Fan, F.W. Williams, Propagation of non-stationary waves along substructural chains, *Journal of Sound and Vibration* 187 (1995) 585–593.
[8] J.H. Lin, W.S. Zhang, F.W. Williams, Pseudo-excitation algorithm for non-stationary random seismic responses, *Engineering Structures* 16 (1994) 270–276.
[9] J.H. Lin, Y.H. Zhang, *Pseudo Excitation Method of Random Vibration*, Science Press, Beijing, 2004 (In Chinese).
[10] W.X. Zhong, J.H. Lin, Q. Gao, The precise computation for wave propagation in stratified materials, *International Journal for Numerical Methods in Engineering* 60 (2004) 11–25.
[11] Q. Gao, W.P. Howson, A. Watson, J.H. Lin, Propagation of non-uniformly modulated evolutionary random waves in stratified viscoelastic solid, Proceedings of the Sixth World Congress on Computational Mechanics in conjunction with the Second Asian-Pacific Congress on Computational Mechanics, Beijing, September 2004. (Full text on CD-ROM of Proceedings.)
[12] D.V. Jones, M. Petyt, Ground vibration in the vicinity of a rectangular load on a half space, *Journal of Sound and Vibration* 166 (1993) 141–159.
[13] D.V. Jones, M. Petyt, *Ground vibration due to a rectangular harmonic load. Journal of Sound and Vibration* 212 (1998) 61–74.
[14] C.J.C. Jones, J.R. Block, Prediction of ground vibration from freight trains, *Journal of Sound and Vibration* 193 (1996) 205–213.
[15] X. Sheng, C.J.C. Jones, M. Petyt, Ground vibration generated by a harmonic load acting on a railway track, *Journal of Sound and Vibration* 225 (1999) 3–28.

[16] X. Sheng, C.J.C. Jones, M. Petyt, Ground vibration generated by a load moving along a railway track, *Journal of Sound and Vibration* 228 (1999) 129–156.
[17] X. Sheng, C.J.C. Jones, D.J. Thompson, A theoretical model for ground vibration from trains generated by vertical track irregularities, *Journal of Sound and Vibration* 272 (2004) 937–965.
[18] H.A. Dieterman, A.V. Metrikine, The equivalent stiffness of a half-space interacting with a beam. Critical velocities of a moving load along the beam,, *European Journal of Mechanics A/Solids* 15 (1996) 67–90.
[19] A.V. Metrikine, K. Popp, Vibration of a periodically supported beam on an elastic half-space, *European Journal of Mechanics A/Solids* 18 (1999) 679–701.
[20] A.V. Vostroukhov, A.V. Metrikine, Periodically supported beam on a visco-elastic layer as a model for dynamic analysis of a high-speed railway track, *International Journal of Solids and Structures* 40 (2003) 5723–5752.
[21] G. Lombaert, G. Degrande, D. Clouteau, Numerical modeling of freefield traffic induced vibrations, *Soil Dynamics and Earthquake Engineering* 19 (2000) 473–488.
[22] W.X. Zhong, The method of precise integration of finite strip and wave-guide problems, *Proceeding of International Conference on Computational Methods in Structural and Geotechnical Engineering*, Hong Kong, December 1994, pp. 51–59.
[23] W.X. Zhong, *The Dual System in Applied Mechanics and Optimal Control*, Kluwer Academic Publishers, Boston, 2004.
[24] B.L.N. Kennett, *Seismic Wave Propagation in Stratified Media*, Cambridge University Press, Cambridge, 1983.
[25] G. Chen, Analysis of random vibration for vehicle and track coupling system, PhD Thesis, South West Jiaotong University, China, 2000. (In Chinese).